C. R. Mecanique 339 (2011) 563–572

Contents lists available at ScienceDirect

Comptes Rendus Mecanique

www.sciencedirect.com

Some considerations about the symmetry and evolution of chaotic Rayleigh–Bénard convection: The flywheel mechanism and the "wind" of turbulence

Marcello Lappa

CTC, Via Salvator Rosa 53, 80046 San Giorgio a Cremano (Na), Italy

ARTICLE INFO

Article history:
Received 13 May 2010
Accepted after revision 5 May 2011
Available online 20 May 2011

Keywords:
Computational fluid mechanics
Thermal convection
Transitions

ABSTRACT

Rayleigh–Bénard convection in finite-size enclosures exhibits really intricate features when turbulent states are reached and thermal plumes play a crucial role in a number of them. This complex mechanism may be regarded as a "machine" containing many different working parts: boundary layers, mixing zones, jets, and a relatively free and isothermal central region. These parts are generally regarded as the constitutive "ingredients" whose interplay leads to the emergence of a macroscopic pattern with well-defined properties. Like the Lorenz model (but with the due differences) such a complex structure has a prevailing two-dimensional nature and can be oriented clockwise or anticlockwise (both configurations are equally likely to occur and the flow can exhibit occasional and irregular "reversals" from one to the other without a change in magnitude). It is usually referred to in the literature as "wind of turbulence" or "flywheel". The present article provides insights into the possible origin of such dynamics and related patterning behavior (supported by "ad hoc" novel numerical simulations carried out for $\mathrm{Pr} = 15$ and $\mathrm{O}(10^3) \leqslant \mathrm{Ra} \leqslant \mathrm{O}(10^{10})$) together with a short exposition of existing theories, also illustrating open points and future directions of research.

1. Introduction

Convection of thermogravitational origin (buoyancy flow) is relevant to several natural and technological contexts. In the geophysical and astrophysical field, for instance, it is worth mentioning convection in Earth's mantle, in Earth's outer core (convection has been also associated with the generation and reversal of Earth's magnetic field, see, e.g., [1] and references therein), and in stars including our sun. Other examples are in the atmosphere (see, e.g., Hartmann et al. [2]), in the oceans (see, e.g., Marshall and Schott [3]), in buildings (see, e.g., Hunt and Linden [4]), in semiconductor technology and in metal-production processes [1,5–8] and a variety of heat transport and mixing problems in other engineering applications (e.g., it enhances heat transport in solar heaters and electronic assemblies) [9–15].

The present review (together with [18], may be regarded as a focused extension of [16] and [17]) illustrates some recent developments in the field of turbulent Rayleigh–Bénard (RB) convection.

In particular, the case of a two-dimensional (2D) square enclosure (heated from below and cooled from above with adiabatic sidewalls, which has become over the years a paradigmatic instance in the study of such phenomena) is considered.

Some attention is also devoted to the historical background and fundamental propaedeutical concepts (as the discussion progresses, the considered configuration is used as a relevant test-bed for assessing the validity of such concepts/models). New (heretofore unseen) considerations/arguments are also developed, which, most remarkably, lead to some general

E-mail address: marlappa@unina.it.

1631-0721/$ – see front matter
doi:10.1016/j.crme.2011.05.002

conclusions concerning the route followed by RB convection in evolving towards chaotic states (and the relationship existing among the transitional stages of evolution it takes in the course of such evolution).

2. Mathematical model and basic assumptions

The simplest model to study the nonlinear dynamics of fluid systems heated from below and cooled from above was the one derived by Lorenz [19] consisting of only three ordinary differential equations, resulting from a hard truncation of a Fourier expansion of the equations of two-dimensional thermal convection. The most important property of this model was the existence of a single clockwise or anticlockwise-oriented convective cell and the appearance of chaos in certain intervals of the system parameters.

It is known, however, that real flow structures exhibit really intricate features when turbulent states are reached and thermal plumes play a crucial role in a number of them [20–24].

Starting from the original Lorenz system of equations, a variety of strategies resorting to the bifurcation analysis of appropriate low-dimensional (simplified) models have been elaborated over the years (see, e.g., [25–27]) in the attempt to capture the fundamental dynamics of such phenomena. In recent years, however, improvements in computer hardware performance have occurred hand in hand with a decreasing hardware cost, which has led to the remarkable possibility of approaching such problems in terms of the Lattice-Boltzmann method (based on kinetic equations and statistical physics [28–30]) and/or direct numerical solution of the classical (continuum mechanics approach) thermal-convection equations (Navier–Stokes and energy equations under the Boussinesq approximation) in their complete (unsteady and nonlinear) form (e.g., [31] and references therein).

Referring time, velocity and temperature to the scales $L^2/\alpha, \alpha/L$ and ΔT, respectively (where α is the thermal diffusivity, L a reference length and ΔT a reference temperature gradient) and scaling all distances on L, such equations in non-dimensional form read

$$\underline{\nabla} \cdot \underline{V} = 0 \tag{1}$$

$$\frac{\partial \underline{V}}{\partial t} = -\underline{\nabla} p - \underline{\nabla} \cdot [\underline{V}\,\underline{V}] + \mathrm{Pr}\,\nabla^2 \underline{V} - \mathrm{Pr}\,\mathrm{Ra}\,T\,\underline{i}_g \tag{2}$$

$$\frac{\partial T}{\partial t} + \underline{\nabla} \cdot [\underline{V} T] = \nabla^2 T \tag{3}$$

where $\underline{i}_g$ is the unit vector along the direction of gravity, Pr the well-known Prandtl number (defined as ν/α where ν is the kinematic viscosity) and Ra the well-known Rayleigh number ($\mathrm{Ra} = g\beta_T \Delta T L^3/\nu\alpha$, β_T being the thermal expansion coefficient).

Paralleling the aforementioned improvement in computer hardware has been the improvement in the efficiency of computational algorithms (and current improvements in hardware cost and computational algorithm efficiency seem to show no obvious sign of reaching a limit, see [1]); most notably, all these factors have combined to make numerical computations increasingly cost effective in the study of turbulent Rayleigh–Bénard convection in contrast to other strategies of analysis.

Here the problem is approached via direct numerical solution (DNS) of Eqs. (1)–(3) with the appropriate boundary conditions (no-slip along the walls, assigned temperatures on the bottom and top plates and no thermal flux through the lateral walls). Following the earlier study of Vincent and Yuen [32], who used 512 grid points per unit (non-dimensional) length to capture the dynamics of turbulent RB convection, in the present study a similar resolution is employed for $\mathrm{Ra} > 10^7$ (600×600 mesh, as also confirmed by a grid-refinement study; the reader is referred to the indication given in the figure captions about the grid for which mesh independence was achieved). The reader may consider Lappa [33] for further details on the primitive-variable approach that has been used for solving numerically Eqs. (1)–(3).

3. The "laminar" flow: bifurcations and symmetry

The considered simple geometrical domain (the cavity with mathematically friendly boundary conditions) is characterized by a high level of intrinsic *symmetry*. Such symmetry, in turn, is a very important ingredient (together with nonlinearity) in pattern formation phenomena.

For a given dynamic system, in general, the governing model equations are invariant under some groups ($\mathcal{G}$) of Euclidean transformations (translations, rotations and reflections of the physical space). Any model equation that is posed on a domain and is invariant under a group $\mathcal{G}$ will inherit those symmetries in $\mathcal{G}$ that preserve the domain and the boundary conditions (symmetries enter into problems of this type from the invariance properties of the governing equations and the shape of the boundary of the considered system, the square container in the present case). Remarkably, the existence of these symmetries implies the possibility of *symmetry breaking*, which is one of the fundamental concepts at the root of phenomena of pattern formation and related evolution towards chaotic behavior.

For the specific case considered here, the distinct modes of convection can be delineated by considering various combinations of the possible symmetries along the horizontal and vertical directions. This leads to partition the set of fundamental modes into four cases, as illustrated in Fig. 1:

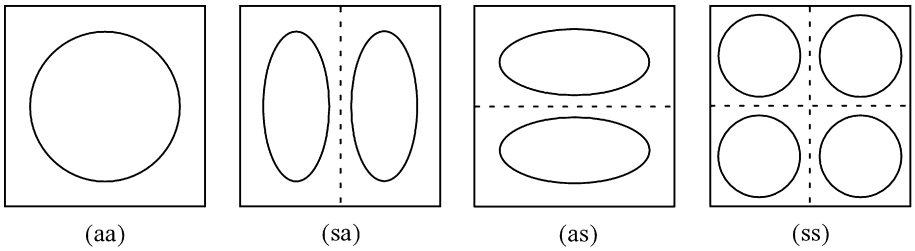

Fig. 1. Categorization of possible solutions of RB convection in 2D finite enclosures in terms of related symmetries.

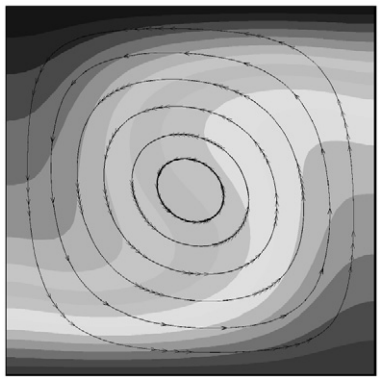

Fig. 2. Steady pattern (temperature distribution and velocity field in the plane (x, y)) of 2D Rayleigh–Bénard convection ($\mathrm{Pr} = 15$, $A = 1$; adiabatic lateral walls) for $\mathrm{Ra} = 1 \times 10^4$ (single-cell flow, grid 100×100).

- (aa): The antisymmetric–antisymmetric mode. This mode has an odd number of vortex cells along both the horizontal (x) and the vertical (y) directions;
- (sa): The symmetric–antisymmetric mode. This mode is characterized by an even number of rolls along the horizontal direction and an odd number of vortices along the y direction;
- (as): The antisymmetric–symmetric mode. This mode exhibits an odd number of rolls along x and an even number of cells in the perpendicular direction;
- (ss): The symmetric–symmetric mode. This mode has an even number of vortex cells along both the horizontal and the vertical directions.

For the square cavity the first bifurcation (convection arising through small localized perturbations of the underlying unstable diffusive background thermal state) occurs at $\mathrm{Ra}_{cr} = 2585$. These perturbations grow in amplitude while, at the same time, invading the unstable background state until nonlinear saturation takes over, leading to a steady state with the (aa) symmetry (Fig. 2).

When the Rayleigh number is sufficiently increased, convection can undergo transition to relatively complex and/or time-dependent regimes. In general, as illustrated by Mizushima and Adachi [34], an initial mode of convection can produce modes with the other symmetries shown in Fig. 1 via a nonlinear interaction mechanism.

Along these lines, Figs. 3 and 4 show some possible steady and oscillatory 2D regimes for the specific case considered here (cavity filled with a silicone oil with $\mathrm{Pr} = 15$) at different values of the Rayleigh number.

As shown in Fig. 4, in particular, for $\mathrm{Ra} = 5 \times 10^5$ the flow becomes oscillatory. One-cell and four-cell flows appear cyclically (in frame (a), the main structure has one diagonal clockwise-oriented cell, in Fig. 4(b) it has four cells, then breaks symmetry again to form one main diagonal counterclockwise-oriented cell).

Basically, due to the symmetry/antisymmetry of the governing equations and of the boundary conditions, different regular solutions appear which can be obtained by reflection about the vertical cavity centreline (parallel to the applied temperature gradient), about the horizontal cavity centreline (perpendicular to the gradient) and about both of them.

For $\mathrm{Ra} \geqslant \mathrm{O}(10^7)$, however, the present numerical simulation shows that the simple (laminar) behavior, with the flow displaying states given by the superposition of a limited number of modes with different symmetries, is lost and the flow becomes turbulent.

In general, turbulent Rayleigh–Bénard convection in enclosures with comparable horizontal and vertical sizes (aspect ratio $A \cong \mathrm{O}(1)$, where A is defined as the ratio of the horizontal to the vertical dimension) produces fields of intense updrafts and downdrafts (rising and descending plumes) that are responsible for much of the vertical heat transport. These structures (sometimes also referred to in the literature as “filaments and patches of thermal anomalies with opposite signs” or simply “thermals”), have horizontal scales comparable to the thicknesses of the boundary layers (BL) in which they arise

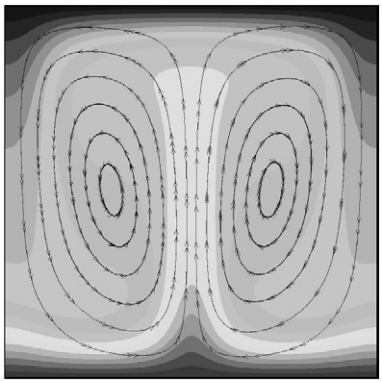

Fig. 3. Steady pattern (temperature distribution and velocity field in the plane (x, y)) of 2D Rayleigh–Bénard convection ($\mathrm{Pr} = 15$, $A = 1$; adiabatic lateral walls) for $\mathrm{Ra} = 1 \times 10^5$ (bicellular flow) (numerical simulations, grid 200×200).

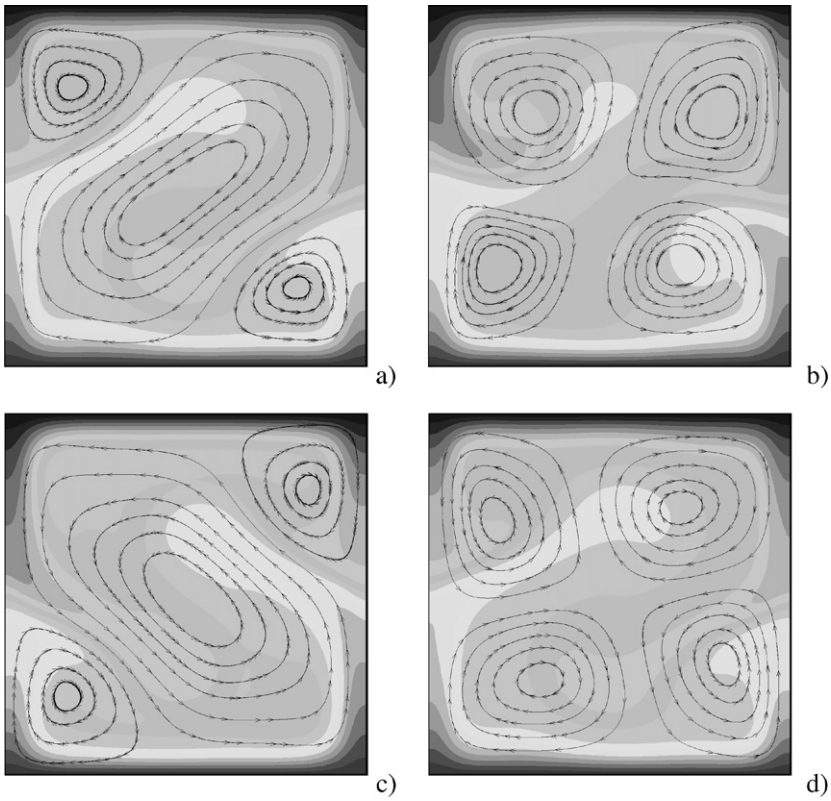

Fig. 4. Snapshots of temperature distribution and related convective cells (plane (x, y)) for 2D oscillatory (periodic) Rayleigh–Bénard convection ($\mathrm{Pr} = 15$, $A = 1$, $\mathrm{Ra} = 5 \times 10^5$): the pattern is shown at $t = 0$ (a), $t = \tau/3$ (b), $t = \tau/2$ (c) and $t = 2\tau/3$ (d) where τ is the time period of the oscillatory phenomenon. The field is featured by a recurrent appearance of one- and four-cell flows (numerical simulation, grid 200×200).

(see, e.g., Parodi et al. [35]). Fig. 5 shows the initial stage of evolution of such a regime for two values of the Rayleigh number.

4. The turbulent flow: results

As time passes, "interaction" between the plumes released by the bottom thermal BL and those released by the top thermal BL occurs and, in spite of the small-scale turbulence (average number of plumes released from the boundary layers) that increases strongly with Ra, the emerging convection pattern retains a large-scale nearly steady structure in which rising and descending "jets" are arranged at well-defined distances (see Figs. 6 and 7).

Hot plumes congregate in an upwelling jet of fluid near the right-hand wall of the container. A similar, downward jet formed from cold plumes occurs on the left-hand wall. Large numbers of hot plumes are also found in left-to-right motion

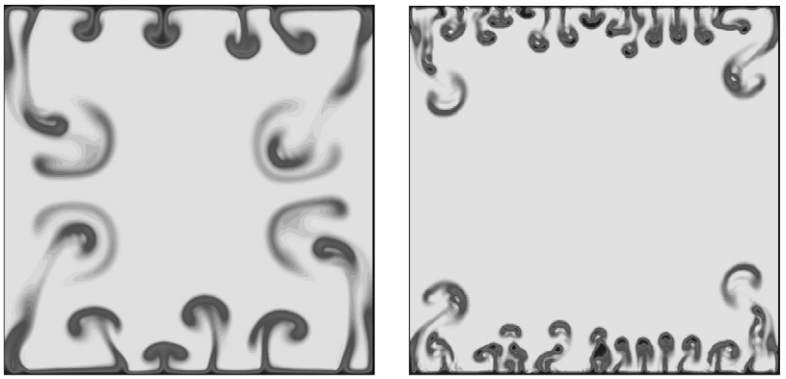

(a) (b)

Fig. 5. Rayleigh–Bénard convection ($\mathrm{Pr} = 15$, $A = 1$; adiabatic lateral walls; numerical simulation, grid 600×600): Early stage of convection with multiple plume-detachment phenomena along the uniformly heated (cooled) bottom (top) wall: (a) $\mathrm{Ra} = 10^8$, (b) $\mathrm{Ra} = 10^9$.

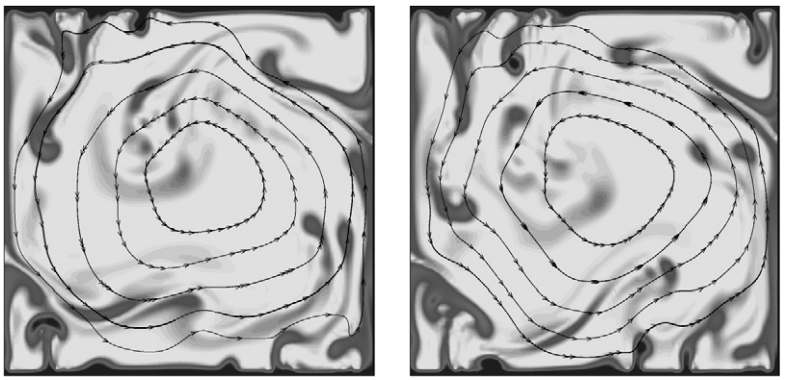

(a) (b)

Fig. 6. Turbulent Rayleigh–Bénard convection ($\mathrm{Pr} = 15$, $A = 1$; $\mathrm{Ra} = 10^8$; adiabatic lateral walls; numerical simulation, grid 600×600): Frames (a) and (b) show the temperature and velocity fields at two close instants during the fully developed regime in which a large-scale coherent circulation (*the wind*) has been established.

in a *mixing zon*e, or viscous boundary layer (kinetic BL), near the bottom of the container. A similar layer on the top contains cold plumes, moving from right to left. The central region contains a few plumes, hot and cold, in a partially random motion. Plumes released from the boundary layers at the bottom hot and upper cold horizontal surfaces, penetrating upwards and downwards towards the opposite wall of lower or higher temperature, cause very intensive mixing in such central region, creating in long-term average an almost isothermal core.

Since, as explained before, the cold and warm plumes are separated laterally in two opposing sidewall regions and exert buoyancy forces to the bulk fluid, an alternating eruption of the thermal plumes, therefore, gives rise to a periodic impulsive torque, which drives a large-scale circulation continuously.

This complex mechanism may be regarded as a "machine" (Kadanoff [36]) containing many different working parts: boundary layers, mixing zones, jets, and a relatively free central region. These parts may be seen as the constitutive "ingredients" whose interplay leads to the emergence of a macroscopic pattern with well-defined properties.

As outlined above and as also demonstrated experimentally (see, e.g., Qiu et al. [37] and Qiu and Tong [38]), the time-averaged flow field maintains, in fact, a large-scale quasi-two-dimensional structure, which rotates in a coherent manner (the moving structures, although highly unsteady, give an ensemble averaged structure pattern very similar to those found in the laminar regime, which have been discussed in Section 3). Like in the Lorenz model (but with the due differences) it has a prevailing two-dimensional nature and can be oriented clockwise or anticlockwise (both configurations are equally likely to occur).

It is usually referred to in the literature as "wind of turbulence" (Grossman and Lohse [39]), simply "wind", "mean wind" (Niemela and Sreenivasan [40]) or "flywheel" (Kadanoff [36]); accordingly, hereafter these terms will be used as synonyms together with "large-scale circulation" (LSC) or motion (Fig. 8).

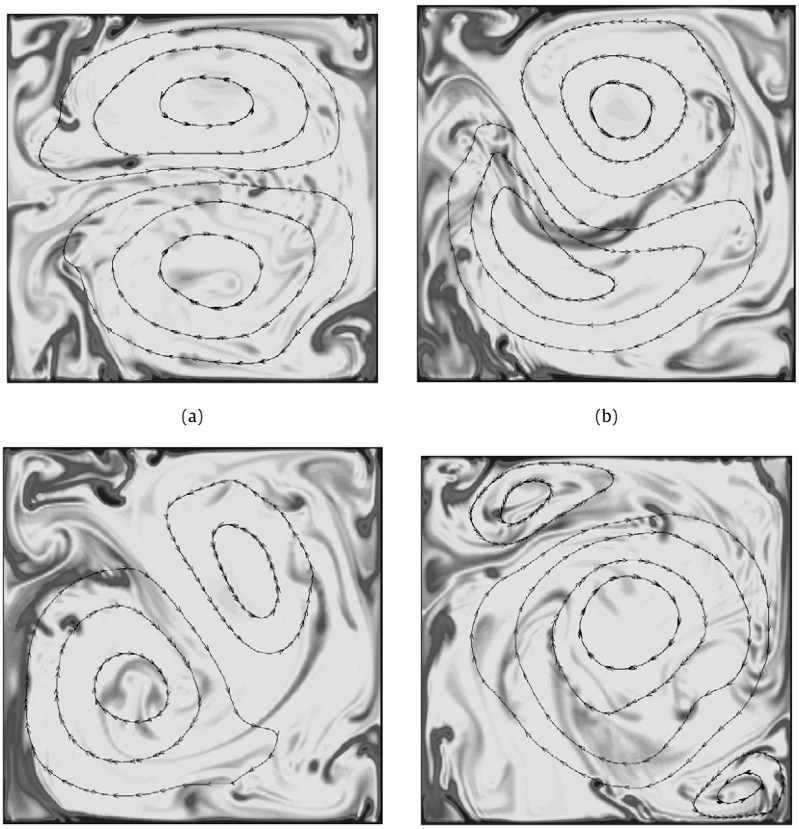

Fig. 7. Turbulent Rayleigh–Bénard convection ($\mathrm{Pr} = 15$, $A = 1$, $\mathrm{Ra} = 10^9$; adiabatic lateral walls; numerical simulation, grid 600×600): Frames from (a) to (d) show the temperature and velocity fields at four different instants.

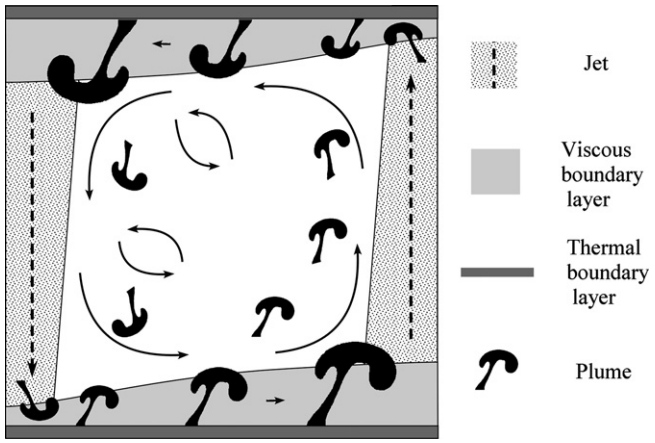

Fig. 8. Sketch of the so-called flywheel mechanism: the spatial organization of the thermal plumes produces a unique flow structure, which undergoes a coherent rotation; plumes evolve from the boundary layers above (below) the bottom (top) plate; first they move laterally toward the sidewall, driven by the prevailing circulation (the horizontal "wind"); they then travel vertically in the region near the sidewall, leaving the central vertical section of the cell relatively free.

This coherent single-roll structure is known to scale with the aspect ratio (see Grossman and Lohse [41]; for aspect ratio unity, the mean wind is comparable in scale to the container size) and with Ra (see, e.g., Qiu and Tong [38], Grossman and Lohse [41], Chillà et al. [42]).

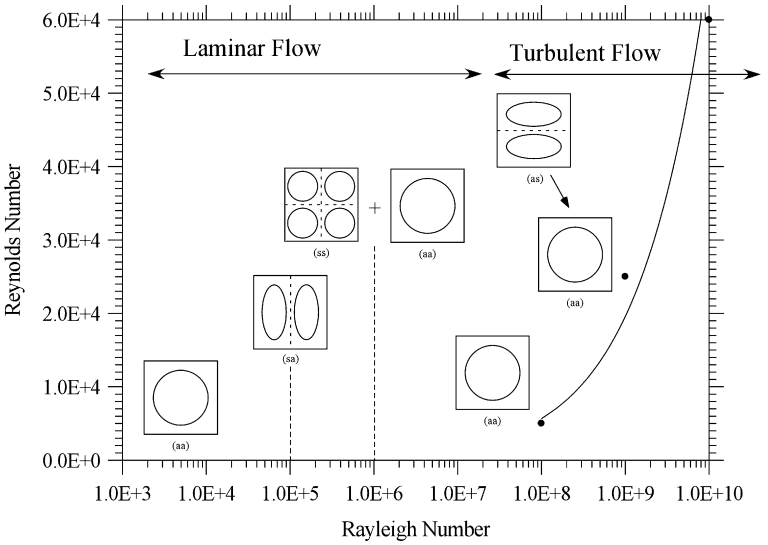

Fig. 9. Reynolds number of the flywheel as a function of the Rayleigh number. The figure also summarizes the symmetry properties (the mode) of the emerging laminar or turbulent mean flow for $\mathrm{Ra} < 10^7$ or $\mathrm{Ra} > 10^7$ respectively.

The present results confirm the general trends provided by experimental investigations with a final self-organized and coherent large-scale motion spanning the height of the container, having a tilted and nearly elliptical shape as evident in Fig. 6 and last frame of Fig. 7.

Whereas such single large-scale flywheel-motion emerges almost immediately for $\mathrm{Ra} = 10^8$, interestingly and in a rather unexpected way, for higher Ra, the transitional stages of evolution (taken by the flow in the course of evolution towards the flywheel) show a transitory pattern with two vertically stacked counter-rotating rolls that has been rarely reported in the literature (only Xi and Xia [43] obtained experimentally a similar mean flow in cylindrical cells with ratio of the diameter to the height 1, 1/2 and 1/3, filled with water and Ra spanning a range of 9.0×10^8–1.9×10^{11}).

For the convenience of the reader, Fig. 9 provides a synthesis of such behavior, together with a plot of the large-scale-flow Reynolds number defined as $U_{\max} L/\nu$ ($U_{\max}$ being the maximum velocity of the wind) as a function of the Rayleigh number (scaling law $\mathrm{Re} \propto \mathrm{Ra}^n$ with $n \cong 0.53$, the reader is referred to the literature for further considerations on this specific aspect).

In line with the existing body of theory, the typical size of the plumes (and of the thermal boundary layers from which they detach) provided by the present simulations decreases as the Rayleigh number increases. This trend, clearly visible in Fig. 5 in which the flywheel (LSC) has not been established yet, has been the subject of intense investigation in the literature together with the analogous problem related to the scaling of the kinetic boundary layers (for a detailed review the reader may consider [17]).

As an example, systematic experimental analyses along these lines where made by Xin et al. [44] and Xin and Xia [45], using the light-scattering technique. They considered a cylindrical cell filled with water and found $\delta_u \propto \mathrm{Ra}^{-0.16}$ (δ_u being the thickness of the kinetic BL) from the velocity profile above the center of the lower plate. Qiu and Xia [46,47] focused on a different geometry (cubic cell), but determined the same scaling exponents found in earlier studies for the cylindrical configuration. Lam et al. [48] extended such studies investigating the Pr dependence over the range $6 \leqslant \mathrm{Pr} \leqslant 1027$ and $2 \times 10^8 \leqslant \mathrm{Ra} \leqslant 2 \times 10^{10}$ ($\delta_u \propto \mathrm{Pr}^{0.24}\,\mathrm{Ra}^{-0.16}$).

Later studies based on the adoption of the particle image velocimetry (PIV) technique led to new and more precise measurements of the velocity field (Sun et al. [49], Xia et al. [50]), including the analysis of the kinetic BLs (Sun et al. [51]).

It is also worth mentioning the numerical simulations by Verzicco and Camussi [52], who (for unity aspect ratio, diameter/height = 1, and $\mathrm{Pr} = 0.7$) provided an area-averaged profile thickness exponent consistent with the Prandtl–Blasius BL theory, i.e. $\delta_u = 0.95 \times \mathrm{Ra}^{-0.23}$. For lower $\mathrm{Pr} = 0.022$ they obtained $\delta_u = 0.1 \times \mathrm{Ra}^{-0.18}$.

Tilgner et al. [53] were the first to measure experimentally also temperature profiles and the thickness of the thermal BL (they considered water, $\mathrm{Pr} = 6.6$, at a fixed $\mathrm{Ra} = 1.1 \times 10^9$). Belmonte et al. [54,55] extended these measurements to the Ra-range $5 \times 10^5 \leqslant \mathrm{Ra} \leqslant 10^{11}$ in compressed air at room temperature ($\mathrm{Pr} = 0.7$).

Lui and Xia [56] measured the lateral dependence of such thickness (δ_T) on the positions in the mean LSC direction and direction perpendicular to the preferred LSC direction in a cylindrical water filled RB cell with unity aspect ratio in the range $2 \times 10^8 \leqslant \mathrm{Ra} \leqslant 2 \times 10^{10}$. Wang and Xia [57] reported similar results for a cubic cell. Most notably, the scaling exponent of δ_T with Ra was found to depend on the position and to vary between -0.35 and -0.28. Lui and Xia [56] found $\delta_T \propto \mathrm{Ra}^{-0.285 \pm 0.004}$ close to the center of the plates (where the thermal BL is thinnest). Xin and Xia [45] and Sun et al. [51] found $\delta_T \propto \mathrm{Ra}^{-0.24}$ and $\delta_T \propto \mathrm{Ra}^{-0.33}$ for $\mathrm{Ra} = \mathrm{O}(10^7$–$10^{11})$ and Ra up to 2×10^{10}, respectively.

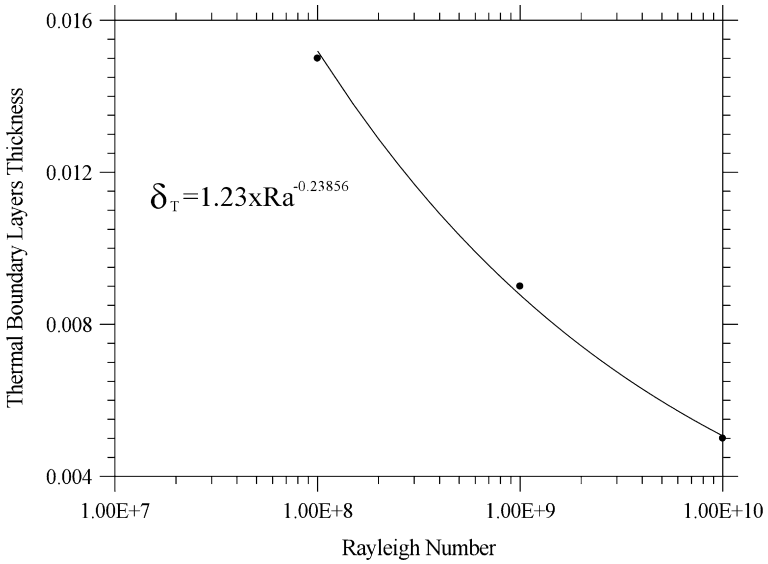

Fig. 10. Non-dimensional thickness of the thermal boundary layer as a function of the Rayleigh number.

Numerical studies expressly focused on the thermal BL thickness are also available. As an example, for unity aspect ratio Verzicco and Camussi [52] obtained for the area-averaged width $\delta_T = 3.1 \times \mathrm{Ra}^{-0.29}$ for $\mathrm{Pr} = 0.7$ over the range $5\times10^5 \leqslant \mathrm{Ra} \leqslant 2 \times 10^7$ and $\delta_T = 2.8 \times \mathrm{Ra}^{-0.25}$ for $\mathrm{Pr} = 0.022$ in the range $5 \times 10^4 \leqslant \mathrm{Ra} \leqslant 10^6$. When going towards the larger Ra regime $2 \times 10^6 \leqslant \mathrm{Ra} \leqslant 2 \times 10^{11}$ Verzicco and Camussi [58] found $\delta_T \propto \mathrm{Ra}^{-0.31}$ for $\mathrm{Pr} = 0.7$ and aspect ratio 1/2. For even larger Ra up to 2×10^{14} Verzicco and Sreenivasan [59] reported $\delta_T \propto \mathrm{Ra}^{-1/3}$ (using water as the working fluid with Rayleigh number Ra in the range from 2×10^8 to 2×10^{10}).

The present results (shown in Fig. 10) are well described by a scaling law of the type $\delta_T \propto \mathrm{Ra}^{-0.24}$ in excellent agreement with the experimental results of Xin and Xia [45] for water and $\mathrm{Ra} = \mathrm{O}(10^7\text{–}10^{11})$.

5. Discussion and conclusion

LSC patterns with a structure resembling the (aa) symmetry or a combination of this symmetry with the (ss) mode (with near-elliptical streamlines displaying the long axis of the ellipse slightly tilted relative to gravity and small counter-rotating vortices positioned near the corners close to the minor axis of the ellipse, more or less prominent depending on Ra, as shown in Figs. 6 and 7(d)), or resembling a combination of the (aa) symmetry with the (as) mode have been clearly observed experimentally (the former described, e.g., by Sun et al. [49], the latter, in particular, reported experimentally by Xi and Xia [43], and numerically here in Fig. 7(a)).

In the light of the considerations developed in the present article supported by "ad hoc" numerical simulations, it becomes fairly evident that for $\mathrm{Pr} > 1$ such large-scale flow should *not* be regarded as a "continuation" of the roll structure observed just after the onset of convection or a continuation of other laminar structures appearing after a secondary or tertiary flow bifurcation of RB convection.

Even though some authors (e.g., Hartlep et al. [60]) have concluded that the flywheel at high Ra may be a reminder of the low-Ra structure, idea supported by the notable similarity between large-scale circulations reported experimentally and almost identical patterning behavior at lower Ra (see, e.g., Figs. 2 and 4), it is opinion of the author of the present article that *there is no kinship between the laminar steady or oscillatory structures at relatively small* Ra *and the mean flow at high* Ra.

Given the peculiar genesis of the large-scale flow, related to a very complex mechanism for high-Pr fluids (by which the ensemble properties of the macroscopic pattern arise from the cooperative behavior of many "parts", i.e. the behavior at large scale arises from detailed structures and interdependencies on a finer scale; the reader is referred, e.g., to the work of Villermaux [61], where it was proposed that the temperature oscillation and related horizontally propagating waves are caused by a thermal boundary layer instability triggered by the incoming thermal plumes from the opposite conducting surface, a mechanism by which the flywheel can be sustained indefinitely), a reasonable rationale for the emergence of such LSC patterns should be inferred from the argument that even in the turbulent regime the system will inherit those symmetries that *preserve the domain, the invariance properties of the governing equations and of the related boundary conditions*.

It is a fairly universally accepted concept that in nature very different systems that are driven out of equilibrium often can show similar patterns although the underlying processes are different. The emergence of a mean flow with a structure that can be classified following the same ideas already used for categorizing the flow arising after the first, second or third bifurcation (when the flow is still laminar) does not mean necessarily that such structure is inherited by preceding stages

of evolution. The numerical simulations for $A = 1$ and $\mathrm{Pr} = 15$ spanning the range $\mathrm{O}(10^3) \leqslant \mathrm{Ra} \leqslant \mathrm{O}(10^{10})$ discussed in the present article provide solid evidence for such a conclusion.

Whether these concepts (no relationship between the structures of the laminar flow and turbulent mean flow) hold also for low-Pr ($\mathrm{Pr} < 1$) fluids (for which the Villermaux theory is no longer applicable) shall be considered as a future direction of research.

References

[1] M. Lappa, Thermal Convection: Patterns, Evolution and Stability, John Wiley & Sons, Ltd., Chichester, England, ISBN 978-0-470-69994-2, 2010, 700 pp.
[2] D.L. Hartmann, L.A. Moy, Q. Fu, Tropical convection and the energy balance at the top of the atmosphere, J. Climate 14 (2001) 4495–4511.
[3] J. Marshall, F. Schott, Open-ocean convection: Observations, theory, and models, Rev. Geophys. 37 (1999) 1–64.
[4] G.R. Hunt, P.F. Linden, The fluid mechanics of natural ventilation – displacement ventilation by buoyancy-driven flows assisted by wind, Building Environm. 34 (1999) 707–720.
[5] K. Achoubir, R. Bennacer, A. Cheddadi, M. El Ganaoui, E. Semma, Numerical study of thermosolutal convection in enclosures used for directional solidification (Bridgman cavity), Fluid Dyn. Mater. Process. 4 (3) (2008) 199–210.
[6] F. Mechighel, M. El Ganaoui, M. Kadja, B. Pateyron, S. Dost, Numerical simulation of three dimensional low Prandtl liquid flow in a parallelepiped cavity under an external magnetic field, Fluid Dyn. Mater. Process. 5 (4) (2009) 313–330.
[7] E.A. Semma, M. El Ganaoui, V. Timchenko, E. Leonardi, Thermal modulation effects on thermosolutal convection in a vertical Bridgman cavity, Fluid Dyn. Mater. Process. 6 (3) (2010) 233–250.
[8] S. Bouabdallah, R. Bessaih, Magnetohydrodynamics stability of natural convection during phase change of molten gallium in a three-dimensional enclosure, Fluid Dyn. Mater. Process. 6 (3) (2010) 251–276.
[9] Md.T. Islam, S. Saha, Md.A.H. Mamun, M. Ali, Two dimensional numerical simulation of mixed convection in a rectangular open enclosure, Fluid Dyn. Mater. Process. 4 (2) (2008) 125–138.
[10] L. Bennamoun, A. Belhamri, Study of heat and mass transfer in porous media: Application to packed-bed drying, Fluid Dyn. Mater. Process. 4 (4) (2008) 221–230.
[11] A.M. Ben-Arous, A.A. Busedra, Mixed convection in horizontal internally finned semicircular ducts, Fluid Dyn. Mater. Process. 4 (4) (2008) 255–262.
[12] G. Accary, S. Meradji, D. Morvan, D. Fougere, Towards a numerical benchmark for 3D low Mach number mixed flows in a rectangular channel heated from below, Fluid Dyn. Mater. Process. 4 (4) (2008) 263–270.
[13] M. El Alami, E.A. Semma, M. Najam, R. Boutarfa, Numerical study of convective heat transfer in a horizontal channel, Fluid Dyn. Mater. Process. 5 (1) (2009) 23–36.
[14] Z. Aouachria, Heat and mass transfer along of a vertical wall by natural convection in porous media, Fluid Dyn. Mater. Process. 5 (2) (2009) 137–148.
[15] A. Meskini, M. Najam, M. El Alami, Laminar mixed heat transfer in a square cavity with heated rectangular blocks and submitted to a vertical forced flow, Fluid Dyn. Mater. Process. 7 (1) (2011) 97–110.
[16] M. Lappa, Secondary and oscillatory gravitational instabilities in canonical three-dimensional models of crystal growth from the melt, Part 1: Rayleigh–Bénard systems, C. R. Acad. Sci. Méc. 335 (5–6) (2007) 253–260.
[17] G. Ahlers, S. Grossmann, D. Lohse, Heat transfer & large-scale dynamics in turbulent Rayleigh–Bénard convection, Rev. Mod. Phys. 81 (2009) 503–537.
[18] M. Lappa, Some considerations about the fundamental properties of Chaotic Rayleigh–Bénard convection: The Lorenz model and the Butterfly effect, FDMP, 2010, in press.
[19] E.N. Lorenz, Deterministic nonperiodic flow, J. Atmospheric Sci. 20 (1963) 130–141.
[20] B.R. Taylor, G. Taylor, J.S. Turner, Turbulent gravitational convection from maintained and instantaneous sources, Proc. R. Soc. Lond. Ser. A 234 (1956) 1–23.
[21] J.S. Turner, Buoyant plumes and thermals, Annu. Rev. Fluid Mech. 1 (1969) 29–44.
[22] T.Y. Chu, R.J. Goldstein, Turbulent convection in a horizontal layer of water, J. Fluid Mech. 60 (1973) 141–159.
[23] B. Castaing, G. Gunaratne, F. Heslot, L. Kadanoff, A. Libchaber, S. Thomae, X. Wu, S. Zaleski, G. Zanetti, Scaling of hard thermal turbulence in Rayleigh–Bénard convection, J. Fluid Mech. 204 (1989) 1–30.
[24] T.H. Solomon, J.P. Gollub, Sheared boundary layers in turbulent Rayleigh–Bénard convection, Phys. Rev. Lett. 64 (1990) 2382–2385.
[25] J.H. Curry, A generalized Lorenz system, Comm. Math. Phys. 60 (3) (1978) 193–204.
[26] R. Festa, A. Mazzino, D. Vincenzi, Lorenz-like systems and classical dynamical equations with memory forcing: An alternate point of view for singling out the origin of chaos, Phys. Rev. E 65 (2002) 046205.
[27] J. Lu, G. Chen, D. Cheng, A new chaotic system and beyond: The generalized Lorenz-like system, Internat. J. Bifur. Chaos Appl. Sci. Engrg. 14 (5) (2004) 1507–1537.
[28] X. Shan, Simulation of Rayleigh–Bénard convection using lattice-Boltzmann method, Phys. Rev. R 55 (1997) 2780–2788.
[29] R. Djebali, M. El Ganaoui, H. Sammouda, R. Bennacer, Some benchmarks of a side wall heated cavity using lattice Boltzmann approach, Fluid Dyn. Mater. Process. 5 (3) (2009) 261–282.
[30] A. Mezrhab, H. Naji, Coupling of lattice Boltzmann equation and finite volume method to simulate heat transfer in a square cavity, Fluid Dyn. Mater. Process. 5 (3) (2009) 283–296.
[31] E. Bucchignani, An implicit unsteady finite volume formulation for natural convection in a square cavity, Fluid Dyn. Mater. Process. 5 (1) (2009) 37–60.
[32] A.P. Vincent, D.A. Yuen, Transition to turbulent thermal convection beyond $\mathrm{Ra} = 10^{10}$ detected in numerical simulations, Phys. Rev. E 61 (5) (2000) 5241–5246.
[33] M. Lappa, On the nature and structure of possible three-dimensional steady flows in closed and open parallelepipedic and cubical containers under different heating conditions and driving forces, Fluid Dyn. Mater. Process. 1 (1) (2005) 1–19.
[34] J. Mizushima, T. Adachi, Sequential transitions of the thermal convection in a square cavity, J. Phys. Soc. Jpn. 66 (1) (1997) 79–90.
[35] A. Parodi, J. von Hardenberg, G. Passoni, E.A. Spiegel, Clustering of plumes in turbulent convection, Phys. Rev. Lett. 92 (2004) 194503.
[36] L.P. Kadanoff, Turbulent heat flow: Structures and scaling, Phys. Today 54 (8) (2001) 34–39.
[37] X.-L. Qiu, S.H. Yao, P. Tong, Large-scale coherent rotation and oscillation in turbulent thermal convection, Phys. Rev. E 61 (6) (2000) R6075–R6078.
[38] X.-L. Qiu, P. Tong, Large-scale velocity structures in turbulent thermal convection, Phys. Rev. E 64 (3) (2001) 036304, 13 pp.
[39] S. Grossman, D. Lohse, Scaling in thermal convection: a unifying theory, J. Fluid Mech. 407 (2000) 27–56.
[40] J.J. Niemela, K.R. Sreenivasan, Rayleigh-number evolution of large-scale coherent motion in turbulent convection, Europhys. Lett. 62 (6) (2003) 829–833.
[41] S. Grossman, D. Lohse, On geometry effects in Rayleigh–Bénard convection, J. Fluid Mech. 486 (2003) 105–114.
[42] F. Chillà, S. Ciliberto, C. Innocenti, E. Pampaloni, Boundary layer and scaling properties in turbulent thermal convection, Nuovo Cimento 15 (1993) 1229–1249.
[43] H.D. Xi, K.Q. Xia, Flow mode transitions in turbulent thermal convection, Phys. Fluids 20 (2008) 055104.
[44] Y.B. Xin, K.-Q. Xia, P. Tong, Measured velocity boundary layers in turbulent convection, Phys. Rev. Lett. 77 (1996) 1266–1269.

[45] Y.-B. Xin, K.-Q. Xia, Boundary layer length scales in convective turbulence, Phys. Rev. E 56 (3) (1997) 3010–3015.
[46] X.L. Qiu, K.-Q. Xia, Viscous boundary layers at the sidewall of a convection cell, Phys. Rev. E 58 (1998) 486–491.
[47] X.L. Qiu, K.-Q. Xia, Spatial structure of the viscous boundary layer in turbulent convection, Phys. Rev. E 58 (1998) 5816–5820.
[48] S. Lam, X.-D. Shang, S.-Q. Zhou, K.-Q. Xia, Prandtl number dependence of the viscous boundary layer and the Reynolds numbers in Rayleigh–Bénard convection, Phys. Rev. E 65 (6) (2002) 066306, 8 pp.
[49] C. Sun, K.Q. Xia, P. Tong, Three-dimensional flow structures and dynamics of turbulent thermal convection in a cylindrical cell, Phys. Rev. E 72 (2005) 026302, 13 pp.
[50] K.-Q. Xia, C. Sun, S.Q. Zhou, Particle image velocimetry measurement of the velocity field in turbulent thermal convection, Phys. Rev. E 68 (2003) 066303.
[51] C. Sun, Y.H. Cheung, K.Q. Xia, Experimental studies of the viscous boundary layer properties in turbulent Rayleigh–Bénard convection, J. Fluid Mech. 605 (2008) 79–113.
[52] R. Verzicco, R. Camussi, Prandtl number effects in convective turbulence, J. Fluid Mech. 383 (1999) 55–73.
[53] A. Tilgner, A. Belmonte, A. Libchaber, Temperature and velocity profiles of turbulence convection in water, Phys. Rev. E 47 (1993) R2253–R2256.
[54] A. Belmonte, A. Tilgner, A. Libchaber, Boundary layer length scales in thermal turbulence, Phys. Rev. Lett. 70 (1993) 4067–4070.
[55] A. Belmonte, A. Tilgner, A. Libchaber, Temperature and velocity boundary layers in turbulent convection, Phys. Rev. E 50 (1994) 269–279.
[56] S.L. Lui, K.-Q. Xia, Spatial structure of the thermal boundary layer in turbulent convection, Phys. Rev. E 57 (1998) 5494–5503.
[57] J. Wang, K.-Q. Xia, Spatial variations of the mean and statistical quantities in the thermal boundary layers of turbulent convection, Eur. Phys. J. B 32 (2003) 127–136.
[58] R. Verzicco, R. Camussi, Numerical experiments on strongly turbulent thermal convection in a slender cylindrical cell, J. Fluid Mech. 477 (2003) 19–49.
[59] R. Verzicco, K.R. Sreenivasan, A comparison of turbulent thermal convection between conditions of constant temperature and constant heat flux, J. Fluid Mech. 595 (2008) 203–219.
[60] T. Hartlep, A. Tilgner, F.H. Busse, Transition to turbulent convection in a fluid layer heated from below at moderate aspect ratio, J. Fluid Mech. 544 (2005) 309–322.
[61] E. Villermaux, Memory-induced low frequency oscillations in closed convection boxes, Phys. Rev. Lett. 75 (1995) 4618–4621.